Understanding redox properties of dinuclear ruthenium(II) complexes by a joint experimental and theoretical analysis

Marie-Pierre Santoni,[a,b,c] *Francesco Nastasi,*[a] *Sebastiano Campagna,**[a] *Garry S. Hanan,**[b] *Bernold Hasenknopf,*[c] *and Ilaria Ciofini**[d]

SUPPLEMENTARY INFORMATION

Table of Contents

Figure S1 - Absorption spectra of **2a** and **2b** in acetonitrile. page S2

Figure S2 - Emission spectra of **2a** and **2b** in acetonitrile. page S2

Figure S3 - Computed orbitals energies (near the HOMO-LUMO gap) and representation of the corresponding molecular orbitals (isocountour value 0.02 au) for the mono-reduced form of complex **2a**. page S3

Figure S4 - Computed orbitals energies (near the HOMO-LUMO gap) and representation of the corresponding molecular orbitals (isocountour value 0.02 au) for the mono-reduced form of complex **2b**. page S4

- Full details of crystallographic data, including Table S1 (X-ray data) page S5-S6

Figure S5 - Linear sweep square wave voltammogram of **2a.** page S7

Figure S6 - Cyclic voltammogram of **2b.** page S8

Figure S7 - Linear sweep square wave voltammogram of **2b.** page S8

Tables S2 and S3 – Redox data from SW voltammograms of **2a** and **2b**. page S9

References page S9

- Full details to Reference 13. page S10

Absorption spectra

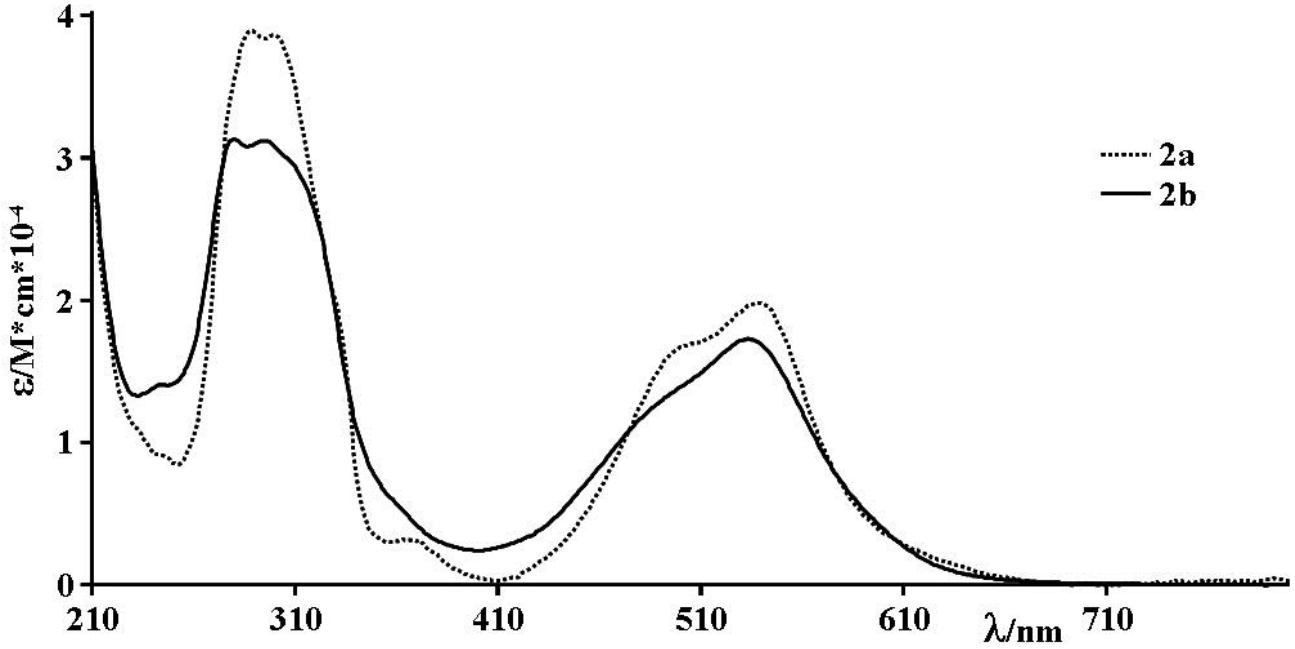

Figure S1. Absorption spectra of **2a** and **2b** in acetonitrile.

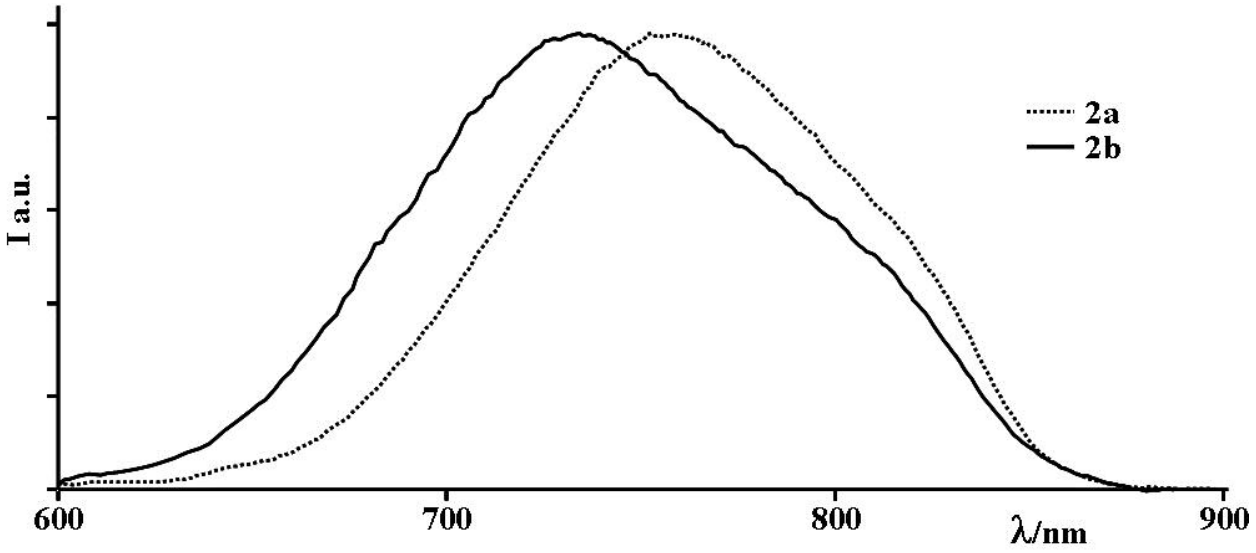

Figure S2 - Emission spectra of **2a** and **2b** in acetonitrile at room temperature.

Computed orbitals

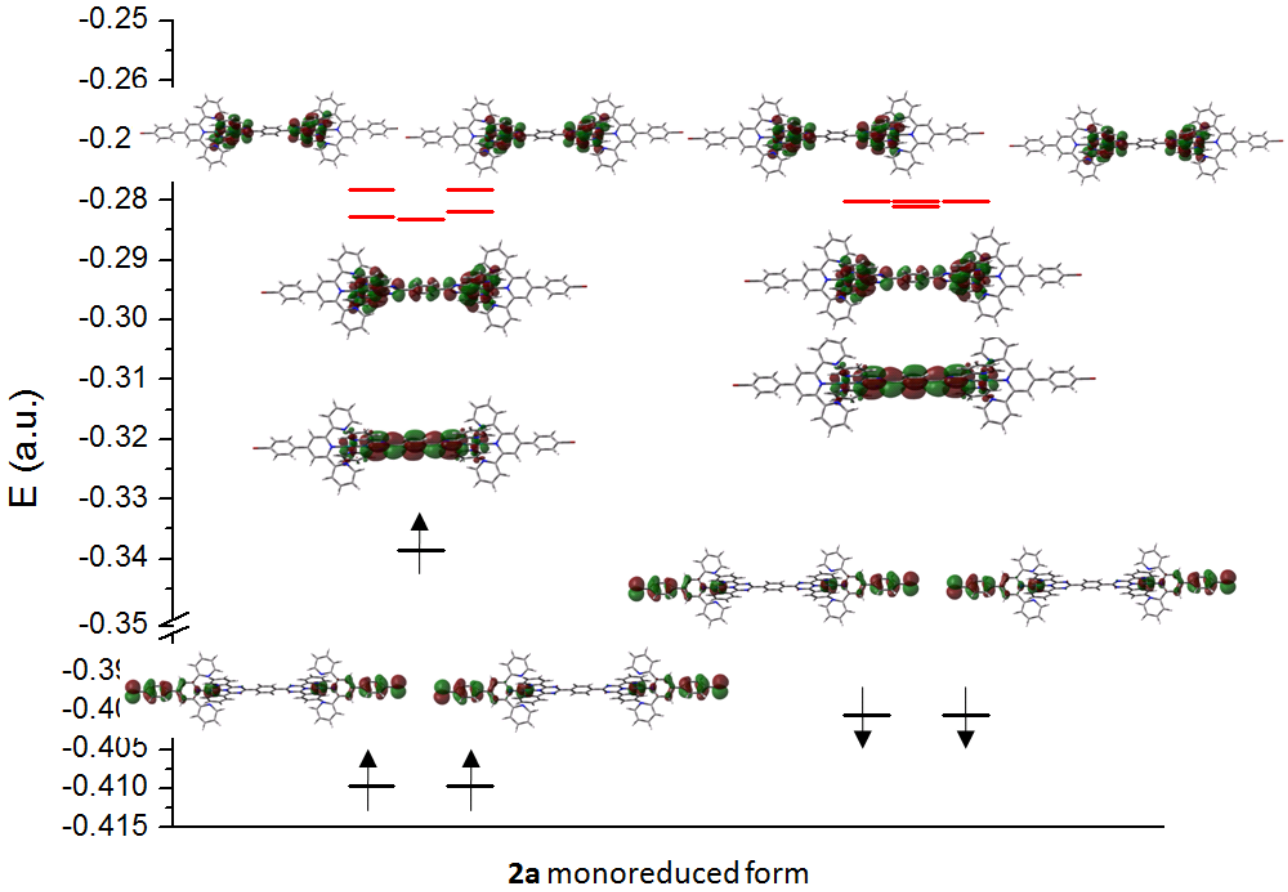

Figure S3 - Computed orbitals energies (near the HOMO-LUMO gap) and representation of the corresponding molecular orbitals (isocountour value 0.02 au) for the mono-reduced form of complex **2a**.

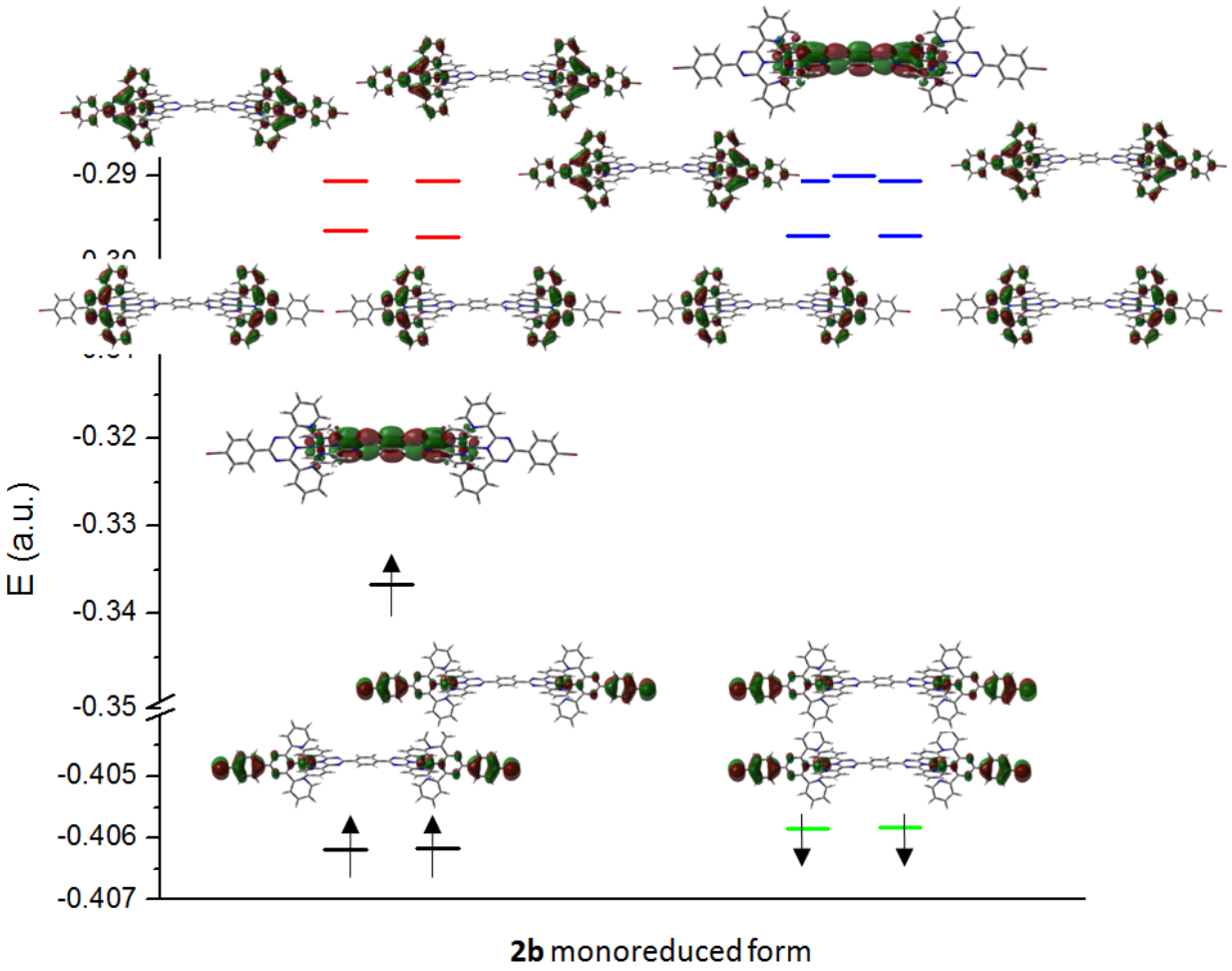

Figure S4. Computed orbitals energies (near the HOMO-LUMO gap) and representation of the corresponding molecular orbitals (isocountour value 0.02 au) for the mono-reduced form of complex **2b**.

X-ray crystallography

Crystallographic data sets were collected from single crystal samples mounted on a loop fibre and coated with N-paratone oil (Hampton Research). The collection was performed using a Bruker Microstar diffractometer equiped with a Platinum 135 CCD Detector, a Helios optics and a Kappa goniometer. The crystal-to-detector distance was 4.0 cm, and the data collection was carried out in 512 x 512 pixel mode. The initial unit cell parameters were determined by a least-squares fit of the angular setting of strong reflections, collected by a 10.0 degree scan in 33 frames over three different parts of the reciprocal space (99 frames total). Due to geometrical constraints of the instrument and the use of copper radiation, we obtain consistently a data completeness lower than 100% in dependence of the crystal system and the orientation of the mounted crystal, even with appropriate data collection routines. Typical values for data completeness range from 83-92% for triclinic, 85-97% for monoclinic and 85-98% for all other crystal systems. Cell refinement and data reduction were performed with SAINT V7.68A (Bruker AXS). Absorption correction was done by multi-scan methods using SADABS96 (Sheldrick). The structure was solved by direct methods and refined using SHELXL97 (Sheldrick).[S1,S2] All non-H atoms were refined by full-matrix least-squares with anisotropic displacement parameters while hydrogen atoms were placed in idealized positions. Refinement of F^2 was performed against all reflections. The weighted R-factor *w*R and goodness of fit S are based on F^2.[S2,S3]

Intensive efforts have been devoted to crystallize hexafluorophosphate salts of all mononuclear and dinuclear complexes, using slow evaporation of concentrated acetonitrile solutions, Et_2O diffusion, layering techniques, without success. Only poor quality single-crystals could be obtained. The compounds either precipitate or tend to form star-shaped packs of very small needles. Any attempt to collect this type of thin needles failed, even using Microstar (Bruker) setup, Cu radiation and increased collection times up to 3 days. Any attempt to collect some thicker needles led to the

obtention of badly twinned data sets, unexpoitable even at low angles. The data set presented (Table S1) is the best one obtained.

Table S1. X-ray data for structures 2a and 3.

Compound	**2a** (Squeeze – see .cif)	**3**
Formula	$[C_{74}H_{48}Br_2N_{16}Ru_2]$	$[C_{55}H_{36}BrN_{11}Ru][PF_6]_2$
M_w (g/mol); F(000)	1523.24 ; 1524	1321.87 ; 1320
T (K); wavelength (Å)	150 ; 1.54178	100 ; 1.54178
Crystal System	Monoclinic	Triclinic
Space Group	P21/c	P-1
Unit Cell: a (Å)	8.7303(8)	9.2589(12)
b (Å)	47.169(4)	14.846(3)
c (Å)	11.5648(11)	21.138(4)
α (°)	90	108.121(8)
β (°)	101.399(4)	98.105(8)
γ (°)	90	93.990(8)
V (Å^3); Z; ; $d_{calcd.}$ (g/cm^3)	4668.5(7) ; 2 ; 1.084	2713.9(7) ; 2 ; 1.618
θ range (°); completeness	1.87 to 57.10; 0.968	2.23 to 54.61; 0.982
collected reflections; R_σ	24576; 0.0630	29410; 0.1072
unique reflections; R_{int}	6125; 0.094	5922; 0.087
μ (mm^{-1}); Abs. Corr.	3.944; Semi-empirical from equivalents	4.562; Semi-empirical from equivalents
$R_1(F)$; w$R(F^2)$ [$I > 2\sigma(I)$]	0.1076; 0.2875	0.1662; 0.3996
$R_1(F)$; w$R(F^2)$ (all data)	0.1357; 0.3049	0.2151; 0.4301
GoF(F^2)	1.074	1.184
Extinction coefficient	0.00109(19)	0.0030(5)
Residual electron density (e$^-$/Å^3)	2.198 and -1.136	2.052 and -1.139

Redox data

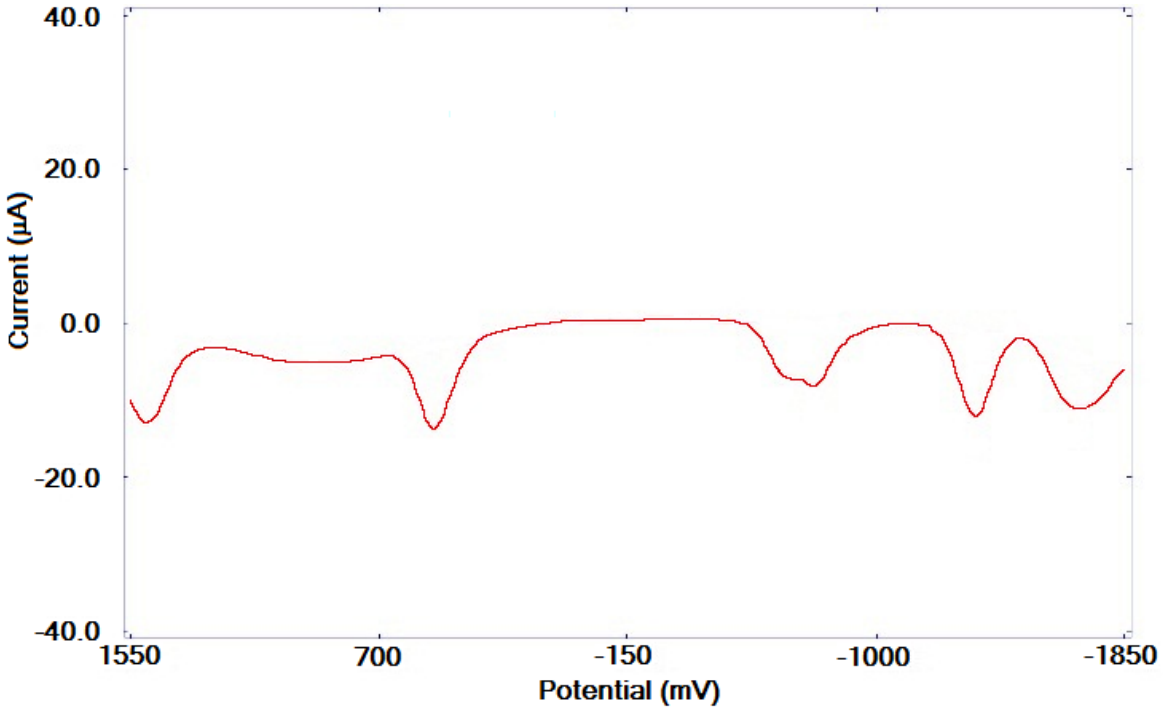

Figure S5. Linear Sweep Square-Wave voltammogram for **2a** and ferrocene in DMF. The oxidation process of Ru(II) is observed (2 metals involved for a total of 2 electrons) and its extrapolated area is used to attribute the number of electrons involved in the reduction processes (see Table S3).

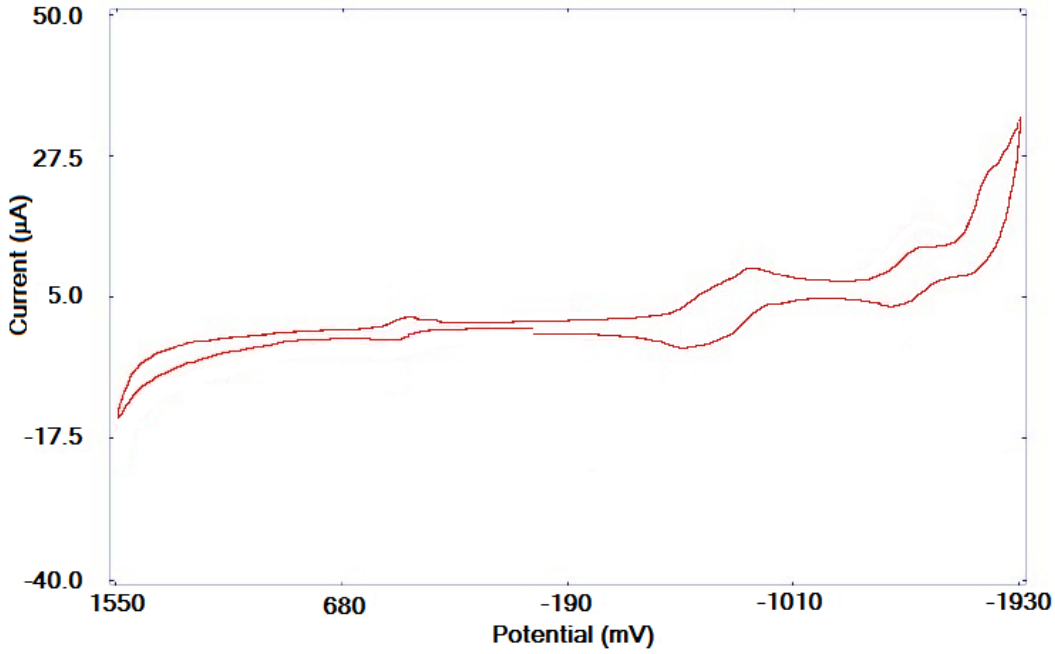

Figure S6. Cyclic voltammogram of **2b** and ferrocene in DMF (scan rate: 100 mV s^{-1}). The oxidations processes in DMF are not observed. They are observed in CH_3CN (not shown here) where the reduction processes remain ill-defined.

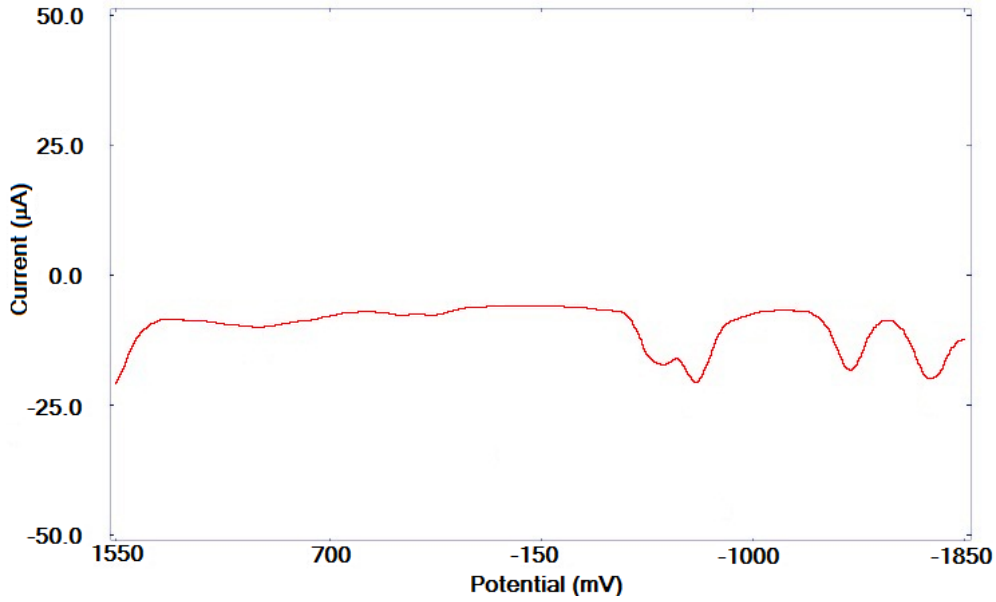

Figure S7. Linear Sweep Square-Wave voltammogram for **2b** in DMF. The oxidation process of Ru(II) is observed (2 metals involved for a total of 2 electrons) and its peak height is used to attribute the number of electrons involved in the reduction processes (see Table S3).

Table S2. Data from the SW voltammogram for **2a**. The ratio between the number of electrons involved in the various processes was based on area ratio.

Potential (V)	+ 1.45	-0.74 and -0.84	-1.38	-1.72
Area (arbitrary units)	1.14	0.90	0.89	1.21
Peak Height (arbitrary units)	1.4	0.7 and 0.8	1.3	1.2
Ratio	**1.0**	0.79	0.79	1.06
Number of e- (assigned)	**2**	1+1	2	2

Table S3. Data from the SW voltammogram for **2b**. The ratio between the number of electrons involved in the various processes was based on peak heights.

Potential (V)	+ 1.50	-0.70 and -0.87	-1.48	-1.80
Area (arbitrary units)	1.31 (extrapolated)	2.89	1.64	1.69
Peak Height (a.u.)	1.80	1.50 and 1.80	1.60	1.70
Ratio	**1.0**	0.83 + 1.00	0.89	0.94
Number of e- (assigned)	**2**	2+2	2	2

References

S1. Sheldrick, G. M. *SHELXS-97, Program for X-ray Crystal Structure Solution* **1997**, Göttingen University, Germany.

S2. Sheldrick, G. M. *Acta Crystallogr. Sect. A* **2008**, 64, 112.

S3. Farrugia, L. J. *J. Appl. Crystallogr.* **1997**, 30, 565.

Full details to Reference 13 (Gaussian 09):

Frisch, M. J.; Trucks, G. W.; Schlegel, H. B.; Scuseria, G. E.; Robb, M. A.; Cheeseman, J. R.; Scalmani, G.; Barone, V.; Mennucci, B.; Petersson, G. A.; Nakatsuji, H.; Caricato, M.; Li, X.; Hratchian, H. P.; Izmaylov, A. F.; Bloino, J.; Zheng, G.; Sonnenberg, J. L.; Hada, M.; Ehara, M.; Toyota, K.; Fukuda, R.; Hasegawa, J.; Ishida, M.; Nakajima, T.; Honda, Y.; Kitao, O.; Nakai, H.; Vreven, T.; Montgomery, Jr., J. A.; Peralta, J. E.; Ogliaro, F.; Bearpark, M.; Heyd, J. J.; Brothers, E.; Kudin, K. N.; Staroverov, V. N.; Kobayashi, R.; Normand, J.; Raghavachari, K.; Rendell, A.; Burant, J. C.; Iyengar, S. S.; Tomasi, J.; Cossi, M.; Rega, N.; Millam, J. M.; Klene, M.; Knox, J. E.; Cross, J. B.; Bakken, V.; Adamo, C.; Jaramillo, J.; Gomperts, R.; Stratmann, R. E.; Yazyev, O.; Austin, A. J.; Cammi, R.; Pomelli, C.; Ochterski, J. W.; Martin, R. L.; Morokuma, K.; Zakrzewski, V. G.; Voth, G. A.; Salvador, P.; Dannenberg, J. J.; Dapprich, S.; Daniels, A. D.; Farkas, Ö.; Foresman, J. B.; Ortiz, J. V.; Cioslowski, J.; Fox, D. J. Gaussian, Inc., Wallingford CT, 2009.